Compression methods for XUV attosecond pulses

Mark Mero,[1] Fabio Frassetto,[2] Paolo Villoresi,[2,3] Luca Poletto,[2] and Katalin Varjú[1,*]

[1]*HAS Research Group on Laser Physics, University of Szeged, 6720 Szeged, Dóm tér 9., Hungary*

[2]*National Research Council of Italy - Institute of Photonics and Nanotechnologies (CNR-IFN), via Trasea 7, 35131-Padova, Italy*

[3]*Department of Information Engineering, University of Padova, via Gradenigo 6/B, 35131-Padova, Italy*

[*]*varju@physx.u-szeged.hu*

Abstract: Attosecond extreme-ultraviolet (XUV) pulses generated in gases via high-order harmonic generation typically carry an intrinsic positive chirp. Compression of such pulses has been demonstrated using metallic transmission filters, a method with very limited tunability. We compare here the compression achievable with a diffraction grating based method with that of metallic filters using simulated high harmonic waveforms in the transmission window of metal films.

OCIS codes: (050.1950) Diffraction gratings; (190.4160) Multiharmonic generation; (260.7200) Ultraviolet, extreme; (320.0320) Ultrafast optics; (320.5520) Pulse compression; (320.5540) Pulse shaping.

References and links

1. Y. Mairesse, A. de Bohan, L. J. Frasinski, H. Merdji, L. C. Dinu, P. Monchicourt, P. Breger, M. Kovacev, R. Taieb, B. Carre, H. G. Muller, P. Agostini and P. Salieres, "Attosecond Synchronization of High-Harmonic Soft X-rays," Science **302,** 1540–1543 (2003).
2. R. Lopez-Martens, K. Varju, P. Johnsson, J. Mauritsson, Y. Mairesse, P. Salieres, M. B. Gaarde, K. J. Schafer, A. Persson, S. Svanberg, C.-G. Wahlstrom, and A. L'Huillier, "Amplitude and Phase Control of Attosecond Light Pulses," Phys. Rev. Lett. **94,** 033001 (2005).
3. E. Gustafsson T. Ruchon, M. Swoboda, T. Remetter, E. Pourtal, R. Lopez-Martens, Ph. Balcou, and A. L'Huillier, "Broadband attosecond pulse shaping," Opt. Lett. **32,** 1353–1355 (2007).
4. A.-S. Morlens, R. Lopez-Martens, O. Boyko, P. Zeitoun, P. Balcou, K. Varju, E. Gustafsson, T. Remetter, A. L'Huillier, S. Kazamias, J. Gautier, F. Delmotte, and M.-F. Ravet, "Design and characterization of extreme-ultraviolet broadband mirrors for attosecond science," Opt. Lett. **31,** 1558–1560 (2006).
5. M. Hofstetter, M. Schultze, M. Fie B. Dennhardt, A. Guggenmos, J. Gagnon, V. S. Yakovlev, E. Goulielmakis, R. Kienberger, E. M. Gullikson, F. Krausz, and U. Kleineberg, "Attosecond dispersion control by extreme ultraviolet multilayer mirrors," Opt. Express **19,** 1767–1776 (2011).
6. M. Hofstetter, A. Aquila, M. Schultze, A. Guggenmos, S. Yang, E. Gullikson, M. Huth, B. Nickel, J. Gagnon, V. S. Yakovlev, E. Goulielmakis, F. Krausz, and U. Kleineberg, "Lanthanum-molybdenum multilayer mirrors for attosecond pulses between 80 and 130 eV," New J. Phys. **13,** 063038 (2011).
7. F. Frassetto, P. Villoresi, and L. Poletto, "Optical concept of a compressor for XUV pulses in the attosecond domain," Opt. Exp. **16,** 6652–6667 (2008).
8. P. Villoresi, "Compensation of optical path lengths in extreme-ultraviolet and soft-x-ray monochromators for ultrafast optics," Appl. Opt. **38,** 6040–6049 (1999).
9. L. Poletto, "Time-compensated grazing-incidence monochromator for extreme-ultraviolet and soft X-ray high-order harmonics," Appl. Phys. B **78,** 1013–1016 (2004).

#154727 - $15.00 USD Received 16 Sep 2011; revised 23 Oct 2011; accepted 23 Oct 2011; published 2 Nov 2011

10. L. Poletto and P. Villoresi, "Time-delay compensated monochromator in the off-plane mount for extreme-ultraviolet ultrashort pulses," Appl. Opt. **45,** 8577–8585 (2006).
11. L. Poletto, P. Villoresi, E. Benedetti, F. Ferrari, S. Stagira, G. Sansone, and M. Nisoli, "Intense femtosecond extreme ultraviolet pulses by using a time-delay-compensated monochromator," Opt. Lett. **32,** 2897–2899 (2007).
12. O. Martinez, "3000 times grating compressor with positive group velocity dispersion: Application to fiber compensation in 1.3-1.6 m region," IEEE J. Quantum Electron. **23,** 59–64 (1987).
13. O. Martinez, "Design of high-power ultrashort pulse amplifiers by expansion and recompression," IEEE J. Quantum Electron. **23,** 1385–1387 (1987).
14. I. Walmsley, L. Waxer, and C. Dorrer, "The role of dispersion in ultrafast optics," Rev. Sci. Instrum. **72,** 1–28 (2001).
15. P. Villoresi, "Harmonic Generation in Gases," Nonlinear Sources: Harmonic Generation in Gases, In: Encyclopedia of Modern Optics, Academic, New York (2004).
16. I. Sola, E. Mevel, L. Elouga, E. Constant, V. Strelkov, L. Poletto, P. Villoresi, E. Benedetti, J.-P. Caumes, S. Stagira, C. Vozzi, G. Sansone, and M. Nisoli, "Controlling attosecond electron dynamics by phase-stabilized polarization gating," Nature Phys. **2,** 319–322 (2006).
17. R. Kienberger, E. Goulielmakis, M. Uiberacker, A. Baltuska, V. Yakovlev, F. Bammer, A. Scrinzi, Th. Westerwalbesloh, U. Kleineberg, U. Heinzmann, M. Drescher, and F. Krausz, "Atomic transient recorder," Nature **427,** 817–821 (2004).
18. G. Sansone, C. Vozzi, S. Stagira, and M. Nisoli, "Nonadiabatic quantum path analysis of high-order harmonic generation: Role of the carrier-envelope phase on short and long paths," Phys. Rev. A **70,** 013411 (2004).
19. M. Lewenstein, Ph. Balcou, M. Yu. Ivanov, A. L'Hullier, and P. B. Corcum, "Theory of high-harmonic generation by low-frequency laser fields," Phys. Rev. A **49,** 2117–2132 (1994).
20. M. Pascolini, S. Bonora, A. Giglia, N. Mahne, S. Nannarone, and L. Poletto, "Gratings in the conical diffraction mounting for an EUV time-delay compensated monochromator," Appl. Opt. **45,** 3253–3562 (2006).
21. J-C. Diels and W. Rudolph, "Ultrashort laser pulse phenomena," Chapter 2.6.2, Academic Press, San Diego (1996).
22. F. Frassetto, P. Villoresi, and L. Poletto, "Beam separator for high-order harmonic radiation in the 3-10 nm spectral region," J. Am. Soc. Am. A **25,** 1104–1114 (2008).

1. Introduction

High-order harmonic generation (HHG) is the prevailing method for the production of ultrashort pulses in the extreme-ultraviolet (XUV) and soft x-ray domains. The broadband coherent harmonic radiation supports optical pulses of attosecond duration. XUV pulses produced via HHG in gases away from the cut-off region typically possess a positive chirp (i.e. the carrier frequency increases with time along the pulse) intrinsic to the generation process [1, 2] leading to longer than transform-limited pulses. Thin metallic filters have constituted a simple and effective way to compensate the intrinsic chirp of XUV pulses [2, 3]. There is, however, a considerable disadvantage: metallic filters exhibit negative group-delay dispersion (GDD) only in narrow, well-defined wavelength regions just above the absorption edge leading to limited spectral tunability. In addition, XUV radiation is strongly absorbed in metallic filters near the absorption edge, which makes it impossible to tune the GDD without changing the losses as well. Reflectors based on the two- and three-layer combination of Mo, Si, B_4C, and La have also been developed and successfully tested for dispersion control in the XUV [4, 5, 6] with a reflectivity of approximately 10% and a bandwidth of 10-13 eV in the center photon energy range of 100-120 eV.

The method presented here provides an alternative for the temporal compression of XUV attosecond pulses by controlling the chirp by means of a conical diffraction grating compressor, what we call the XUV attosecond compressor (XAC) [7]. The design of the XAC originates from the scheme of an XUV time-delay compensated monochromator [8, 9, 10, 11] realized to select a suitable portion of the broadband HH spectrum without altering the intrinsic temporal pulse shape. The method aims to solve the problem of temporal compression of broadband XUV attosecond pulses by exploiting the influence on the pulse phase of a double-grating compressor. The method is well consolidated for the use in many ultrafast devices in the visible and near infrared, as it was demonstrated that grating pairs may be arranged to realize compensators

#154727 - $15.00 USD Received 16 Sep 2011; revised 23 Oct 2011; accepted 23 Oct 2011; published 2 Nov 2011

for laser cavity dispersion, phase modulators, stretchers and compressors for chirped pulse amplification [12, 13, 14]. The XAC design extends to the XUV spectral range the use of gratings to control the phase of the pulse by means of the conical diffraction geometry.

We test here the applicability of the grating-based pulse shaper on simulated HH radiation and compare its pulse compression capability to that of aluminum and zirconium filters in wavelength regions, where these metal films are transparent.

2. Synthesis of an attosecond pulse

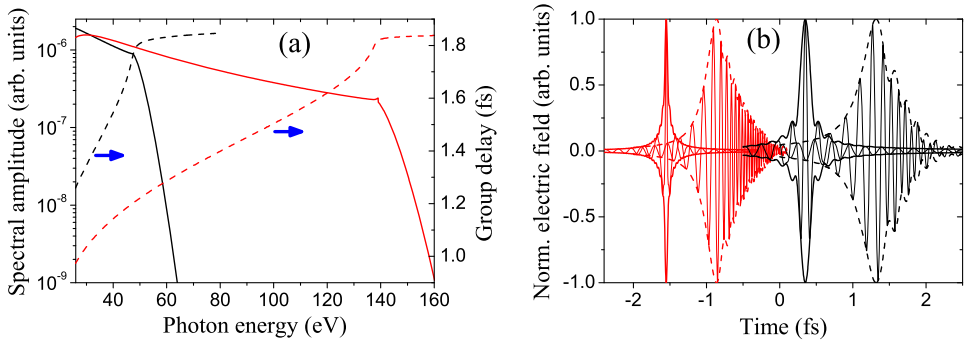

Fig. 1. (a) Spectrum and group delay of the high-order harmonic radiation produced at a generating intensity of 1.5×10^{14} W/cm^2 in argon (black lines) and 6×10^{14} W/cm^2 in neon (red lines). (b) Corresponding attosecond pulses possessing an intrinsic chirp (dashed lines) and their Fourier limit (solid lines). For better clarity, the pulses are shifted in time with respect to each other.

High-order harmonic generation in rare gases is a result of an electronic process: after optical ionization, the electron is accelerated in the laser field, then recaptured by the parent ion emitting its excess energy in form of an XUV photon. The properties of the radiation is inherited from the electron. Using multi-cycle laser pulses for the generation process, a sequence of spectral peaks at odd multiples of the fundamental frequency is produced, which corresponds to a series of attosecond pulses separated by half of the fundamental period in the time domain [15]. On the other hand, HHG with few-cycle pulses combined with ellipticity [16] or intensity gating [17] limits harmonic emission to a single half-cycle leading to the production of an isolated attosecond pulse, i.e. a selection of one pulse from the train.

The quantum mechanical description of the generation process makes use of certain simplifications, such as the one-electron and strong field approximations. The simulated XUV fields presented in this paper are calculated via a nonadiabatic version [18] of the saddlepoint method [19]. In the simulation, we consider a 25-fs, Gaussian sine-type driving pulse at a center wavelength of 790 nm. HHG is numerically limited to the first half cycle after the peak to produce continuous spectra and group delay (GD) curves. The modeling was performed for two generating peak intensities, 1.5×10^{14} W/cm^2 for argon and 6×10^{14} W/cm^2 for neon, leading to HH spectra in the transmission windows of Al and Zr, respectively.

As shown in Fig. 1(a), the cutoff frequency increases, while the intrinsic chirp (i.e. the slope of the GD curves) decreases with increasing generating intensity. The combination of XUV chirp and bandwidth in our case is such that the emerging XUV pulses are shorter, when the generating intensity is higher, c.f. Fig. 1(b). We synthesize the attosecond pulses from short trajectory components, since this is the part of the generated radiation that survives propagation in the generating medium.

#154727 - $15.00 USD Received 16 Sep 2011; revised 23 Oct 2011; accepted 23 Oct 2011; published 2 Nov 2011

3. Compression by metallic filters

Anomalous dispersion near absorption resonances can be exploited to compensate the positive chirp of the generated attosecond pulses. By matching the generating intensity to the material properties, one can achieve compression of attosecond pulses close to the Fourier limit [2, 3].

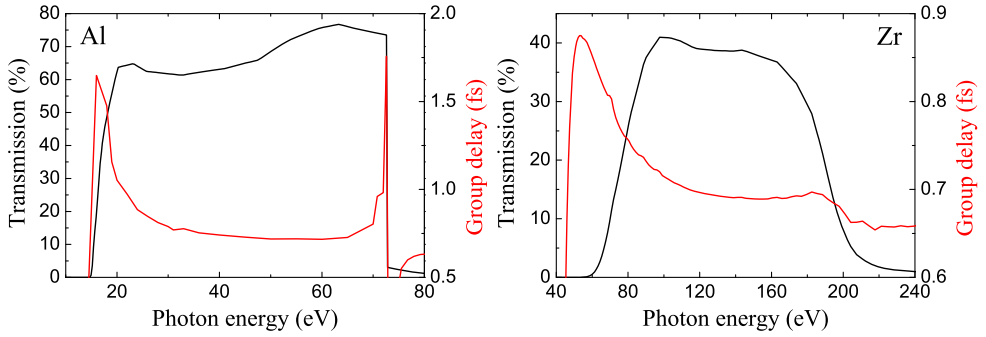

Fig. 2. Transmission (black lines) and group delay (red lines) of a 200-nm-thick aluminum (left) and zirconium (right) filter as a function of photon energy.

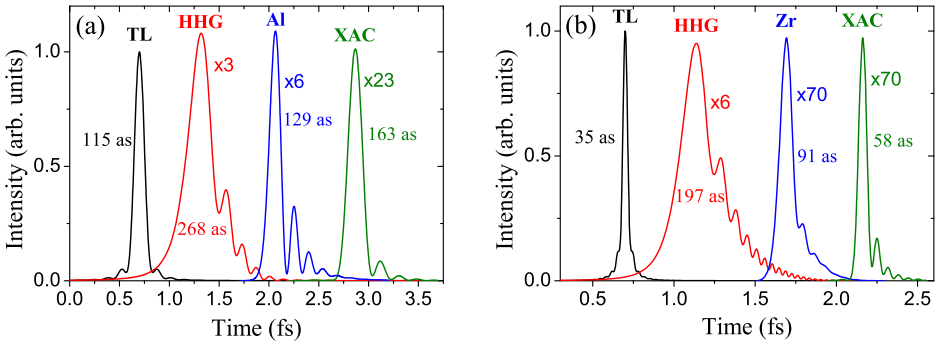

Fig. 3. Attosecond pulse generated at (a) 1.5×10^{14} W/cm^2 and (b) 6×10^{14} W/cm^2. The FWHM duration values are indicated in the graph. TL: transform limited, HHG: right after high harmonic generation, Al: after a 600-nm Al film, Zr: after a 250-nm Zr film, XAC: after an XUV grating compressor with parameters given in the text. For better clarity, the pulses are shifted in time with respect to each other.

As shown in Fig. 2, aluminum filters transmit in the 20-70 eV region and possess a negative GDD at the onset of transmission. A laser pulse with a peak intensity of 1.5×10^{14} W/cm^2 generates high harmonics in argon approximately in this spectral range. By properly choosing the thickness of the filter, one can minimize the GDD. However, the transmission of metal films depends on the added GDD. The shortest pulse duration for the simulated radiation of 129 attosecond (asec) is obtained at an aluminum thickness of 600 nm. The transform limited duration at full width at half maximum (FWHM) is 115 asec. The peak intensity after the filter is reduced by a factor of 6 compared to the peak intensity of the bandwidth limited pulse, which is normalized in Fig. 3(a). The asymmetric side structures are due to the higher order residual chirp still present after the filter.

#154727 - $15.00 USD Received 16 Sep 2011; revised 23 Oct 2011; accepted 23 Oct 2011; published 2 Nov 2011

Zirconium works as a bandpass filter in the 70-200 eV region, which is sufficiently large for the high harmonic range generated at a laser intensity of 6×10^{14} W/cm^2. The shortest pulse duration of 71 asec is achieved at a Zr thickness of 1150 nm with an intensity reduction of a factor of 4600 compared to that of the bandwidth limited pulse. The transmission is comparable to that of the XAC at a thickness of 250 nm (c.f. Fig. 3(b)), which does not allow compression to much below 3 times the bandwidth limit. The transform limited pulse duration is 35 asec.

4. Compression by an XUV attosecond compressor

The XAC design uses the gratings in the conical diffraction mount, since it has been demonstrated that such a geometry gives a remarkable improvement both in throughput and tunability in the XUV with respect to the classical diffraction mount [20]. The conical diffraction or off-plane mount is shown in Fig. 4, where the direction of the incoming rays is described by two parameters: the altitude γ and the azimuth α angles. All the rays leave the grating at the same altitude at which they approach it. The azimuth α of the incoming rays is defined to be zero, if the rays lie in the plane perpendicular to the grating surface and parallel to the grooves. Therefore, $-\alpha$ is the azimuth of the zeroth-order beam. $\beta(\omega)$ is the azimuth of the diffracted beam at angular frequency ω. The grating equation for conical diffraction is written as,

$$\sin\gamma(\sin\alpha + \sin\beta(\omega)) = m\lambda(\omega)\sigma, \tag{1}$$

where σ is the groove density, m is the diffraction order, and λ is the wavelength.

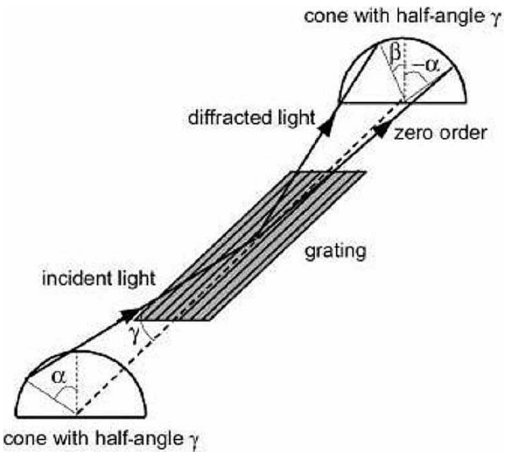

Fig. 4. Grating in the off-plane mount. α: azimuth angle, γ: altitude angle.

The basic version of the XAC arrangement is directly related to the well-known double-grating design in the classical diffraction mount for the visible and near-infrared. It consists of two identical plane gratings mounted in the conical diffraction geometry and aligned at the same altitude, as shown in Fig. 5(a). The azimuth angle α_1 of the incident rays on the first grating G1 is the same for all wavelengths. The highest diffraction efficiency for $m = 1$ is reached at the blaze wavelength $\lambda_B = 2\sin\gamma\sin\delta/\sigma$ at $\beta_1(\lambda_B) = \alpha_1 = \delta$, where δ is the blaze angle. The azimuth angle $\beta_1(\lambda)$ of the rays diffracted from G1 is calculated using Eq. (1). The beam propagates toward the second grating placed at a normal distance h. Due to the symmetry of the configuration, the azimuth angle of the rays diffracted from G2 is independent of wavelength, $\beta_2(\lambda) = \alpha_1$, leading to parallel exit rays. By adapting the method described in Ref. [21], one

#154727 - $15.00 USD Received 16 Sep 2011; revised 23 Oct 2011; accepted 23 Oct 2011; published 2 Nov 2011

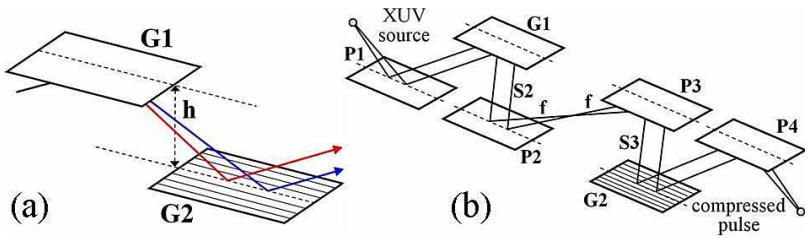

Fig. 5. (a) Schematic of the XAC based on two plane conical diffraction gratings at a normal distance *h*. (b) More detailed view of the XAC. G1 (G2): diffraction grating 1 (2), P1, ..., P4: parabolic mirrors, *S*2 (*S*3): distance between G1 and P2 (P3 and G2), f: focal length of P2 and P3.

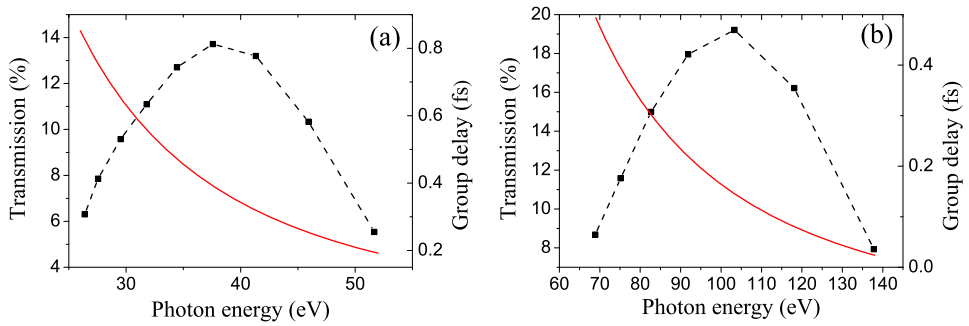

Fig. 6. Transmission spectra (black) and group delay (red) of XACs as a function of photon energy. (a) $\sigma = 100\,\mathrm{mm}^{-1}$, $\alpha = 3.7°$, $\gamma = 1.5°$, $h = 600\,\mu$m, (b) $\sigma = 200\,\mathrm{mm}^{-1}$, $\alpha = 4.14°$, $\gamma = 1°$, $h = 500\,\mu$m. Carbon coatings are assumed in the calculations. The transmission windows are limited to one octave as explained in the text. The dashed lines are guides to the eye.

can derive an analytic formula for the spectral phase introduced by the two grating arrangement for on-axis rays in a single pass,

$$\begin{aligned}\Psi(\omega) &= \frac{\omega h}{c\sin\gamma\cos\beta(\omega)}\left\{1+\cos\left[\pi-\cos^{-1}\left(\sin^2\gamma\cos(\alpha-\beta(\omega)+\pi)+\cos^2\gamma\right)\right]\right\} \\ &- 2\pi h\sigma\tan\beta(\omega), \end{aligned} \tag{2}$$

where *c* is the velocity of light. Differentiation of Eq. (2) with respect to ω yields the GD, GDD, third-order dispersion, etc., curves. The formula proves that the GD and GDD are proportional to the grating distance, as was speculated in Ref. [22]. It is important to note that Eq. (2) yields the spectral phase only for the chief ray and does not account for aberrations. However, it allows for a quick optimization of grating compressor parameters for best chirp compensation.

Unfortunately, the configuration with plane gratings shown in Fig. 5(a) is not suitable for pulse compression in the XUV, since the distance *h* that is required to give the necessary GDD that compensates for the intrinsic pulse chirp is too small to be realized in practice. Therefore, the plane grating configuration of Fig. 5(a) has been modified as shown in Fig. 5(b), adapted from Ref. [7]. The design consists of six optical elements, namely four identical parabolic mirrors (P1-P4) and two identical plane gratings (G1, G2). The parabolic mirrors are used in grazing incidence to collimate and refocus the XUV radiation with negligible aberrations. Therefore, the gratings are illuminated in parallel light. The XUV source is located in the front

#154727 - $15.00 USD Received 16 Sep 2011; revised 23 Oct 2011; accepted 23 Oct 2011; published 2 Nov 2011

focal plane of P1 and the rays are collected at the focus of the last parabolic mirror P4. In contrast to traditional grating compressors used for ultrashort pulses [21], our arrangement uses only a single pass through the grating compressor and the different frequency components overlap only in the back focal plane. A spectrally dispersed image of the source is obtained in the intermediate plane, where a slit is placed to block diffracted orders with $m \geq 2$. Note that due to the slit, the bandwidth of the XAC is limited to one octave.

The two focusing mirrors placed between the gratings act as a telescopic arrangement reducing the effective path between the gratings. This makes it possible to (i) produce an effectively negative grating separation with positive GDD, (ii) continuously tune the GDD from negative to positive values, and (iii) achieve the exceedingly small grating separations necessary for compensation of HH chirp. It has been demonstrated in Ref. [7] that the condition for zero-dispersion is $S-2f=0$, where $S=S2+S3$. Since f is fixed, the GDD introduced by the XAC depends only on S, that is the only parameter to be tuned. Once the parameter h that is required for compensation has been calculated from Eq. (2), the effective XAC displacement from the zero-dispersion case is calculated as $\Delta S = S-2f = h/[\sin\gamma\cos\beta(\omega_0)]$ with ω_0 being the center angular frequency. It can be noted that the mechanical design of the XAC is simplified, if S2 is kept fixed and S3 is finely tuned to change the GDD. A suitable value for f is in the range of 150-250 mm, making the total envelope of the XAC of the order of one meter.

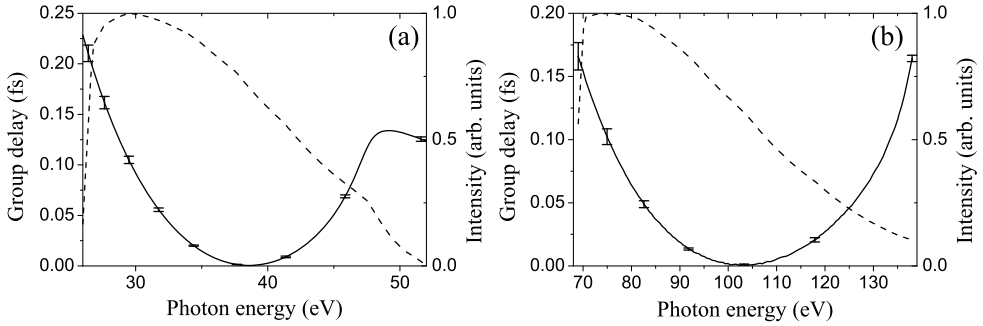

Fig. 7. Residual GD of the attosecond pulses after the XAC generated at peak intensities of (a) 1.5×10^{14} W/cm^2 and (b) 6×10^{14} W/cm^2. The corresponding spectra after chirp compensation by the XACs are shown by the dashed lines on the right axes. The error bars indicate the FWHM spread in GDs due to the aberration of the system.

The XUV grating compressor must be designed for each spectral range in order to maximize the total throughput and minimize the spread of optical pathlengths due to aberrations. A ray tracing simulation was used to find the optimal grating parameters that minimize aberrations following the procedure described in Ref. [7]. As the bandwidth of the XAC is limited to one octave, a range has to be chosen from the XUV spectrum for which the XAC is to be optimized. For the generating intensity of 1.5×10^{14} W/cm^2 and 6×10^{14} W/cm^2, we chose the photon energy regions of 26-52 eV and 69-138 eV, respectively.

In the lower generating intensity case, the optimal grating parameters are $\sigma = 100$ mm^{-1}, $\alpha = 3.7^\circ$, and $\gamma = 1.5^\circ$. The pulse duration was minimized using Eq. (2) leading to a value of $h = 0.6$ mm, corresponding to a value $\Delta S = 22.8$ mm. The olive curves in Fig. 3(a) show the pulses in the temporal domain after the XAC. The asymmetric satellites are a result of higher order chirp still present after the XAC. The compressed pulse duration is 163 asec, which is approximately 25% longer than the duration obtained using an Al filter at a lower loss level. The transmission spectrum of the XAC including the efficiency of the 2 gratings and 4 paraboloidal

#154727 - $15.00 USD Received 16 Sep 2011; revised 23 Oct 2011; accepted 23 Oct 2011; published 2 Nov 2011

reflectors is shown in Fig. 6(a). The grating efficiency has been calculated following the method described in Ref. [20]. Carbon coatings were assumed in the calculations, which exhibit an almost constant reflectivity of 93% for s-polarized light at an angle of incidence of 87^o in the photon energy range of 20-140 eV. The sharp edges in the spectrum are due to the intermediate slit that blocks higher order diffracted beams in the compressor. Figure 7(a) shows the residual GD and the spectrum after the XAC together with the spread of pathlenghts due to aberrations as a function of photon energy. The FWHM spread values are ≤ 16 asec in the whole spectral range, which is sufficiently small compared to the compressed pulse duration.

In the higher generating intensity case, the optimal grating parameters in terms of aberrations and pulse duration are $\sigma = 200$ mm^{-1}, $\alpha = 4.14^\circ$, and $\gamma = 1^\circ$. The transmission spectrum of the XAC is shown in Fig. 6(b). The shortest pulse duration of 58 asec was reached at a normal grating distance of $h = 0.5$ mm, corresponding to a value $\Delta S = 28.7$ mm. The minimum compressed pulse duration is almost a factor of two shorter than the duration obtained using a Zr filter at the same level of losses. The normalized spectrum and the residual GD after the XAC are shown in Fig. 7(b). The FWHM spread values are ≤ 22 asec in the whole spectral range, which is less than half of the minimum compressed pulse duration.

We note that tuning the ratio of third-order and second-order dispersion by varying the XAC parameters is possible, but limited, as the tolerances on the azimuth and altitude angles that provide an acceptable level of aberrations are relatively high [7].

5. Conclusions

We have compared the performance of Al and Zr filters and conical diffraction grating compressors to compress XUV attosecond pulses in spectral regions, where the metal filters are transparent. We found that the performance of the XUV attosecond compressor (XAC) in terms of the shortest pulse duration and highest intensity achievable is poorer than that of aluminum films in the photon energy range of 39 ± 13 eV and better than that of zirconium films in the 103 ± 34-eV range. In general, XACs are more versatile than metal filters even in the transparency range of metals. Aberrations in XACs can introduce lengthening of the pulses by a few 10% compared to the minimum duration of the aberrationless system. In contrast to metal filters, XACs allow continuous tunability of the group delay dispersion from negative to positive values with a throughput that is independent of the amount of GDD introduced. Outside the transparency range of metal filters, XACs provide a unique pulse shaping capability. The intermediate plane in the XAC arrangement, where the radiation is spectrally dispersed, may enable further pulse shaping capability with the use of a deformable mirror.

In comparison to XUV chirped mirrors, XACs can in principle provide lower losses, much larger bandwidths, and more flexible chirp control. While currently available state-of-the-art XUV chirped mirrors exhibit only ± 0.01 fs^2 per bounce at a reflectivity of $\sim 10\%$ and a bandwidth of only $\sim 10\%$ of the center wavelength [6], XACs can in principle provide GDDs $\gg 0.01$ fs^2 and reflectivities well above 10% at bandwidths approaching one octave. The advantages of using XACs are more pronounced in the photon energy range above 100 eV, where the availability of materials for chirped mirrors is limited. However, considerably simpler, more compact, and much less alignment sensitive experimental setup is possible with the use of an XUV chirped mirror than with an XAC.

Acknowledgments

KV acknowledges the support of an OTKA/NKTH grant (H07B 74250) and the Bolyai Postdoctoral Fellowship. The project was partially funded by "TÁMOP-4.2.1/B-09/1/KONV-2010-0005 - Creating the Center of Excellence at the University of Szeged" supported by the European Union and co-financed by the European Social Fund. The project was partially funded by

"FIRB SERAPIDE - Single Electron Recollision for intense Attosecond Pulses and Investigation of the Dynamics of Electron wavepackets" supported by the Italian Ministry for Education, University and Research.

#154727 - $15.00 USD Received 16 Sep 2011; revised 23 Oct 2011; accepted 23 Oct 2011; published 2 Nov 2011